

Review

Progress on Noble-Metal-Free Organic–Inorganic Hybrids for Electrochemical Water Oxidation

Zheng Tan ¹, Lihua Zhang ^{1,2}, Tong Wu ^{1,2}, Yinbo Zhan ^{1,2}, Bowei Zhou ¹, Yilin Dong ^{1,2} and Xia Long ^{1,*}

¹ China-UK Low Carbon College, Shanghai Jiao Tong University, Shanghai 200240, China; a.j.fikrytan@sjtu.edu.cn (Z.T.); qlwlym@sjtu.edu.cn (L.Z.); wt1996@sjtu.edu.cn (T.W.); zhanyinbo@sjtu.edu.cn (Y.Z.); bowei_sjtu@sjtu.edu.cn (B.Z.); 17805425648@sjtu.edu.cn (Y.D.)

² School of Mechanical Engineering, Shanghai Jiao Tong University, Shanghai 200240, China

* Correspondence: x.long@sjtu.edu.cn

Abstract: Emerging as a new class of advanced functional materials with hierarchical architectures and redox characters, organic–inorganic hybrid materials (OIHs) have been well developed and widely applied in various energy conversion reactions recently. In this review, we focus on the applications and structure–performance relationship of OIHs for electrochemical water oxidation. The general principles of water oxidation will be presented first, followed by the progresses on the applications of OIHs that are classified as metal organic frameworks (MOFs) and their derivatives, covalent organic framework (COF)-based hybrids and other OIHs. The roles of organic counterparts on catalytic active centers will be fully discussed and highlighted with typical examples. Finally, the challenges and perspectives assessing this promising hybrid material as an electrocatalyst will be provided.

Keywords: organic–inorganic hybrid; water oxidation; electrochemical catalysis



Citation: Tan, Z.; Zhang, L.; Wu, T.; Zhan, Y.; Zhou, B.; Dong, Y.; Long, X. Progress on Noble-Metal-Free Organic–Inorganic Hybrids for Electrochemical Water Oxidation. *Inorganics* **2023**, *11*, 424. <https://doi.org/10.3390/inorganics11110424>

Academic Editors: Francis Verpoort, Claudio Pettinari, Maurizio Peruzzini, Richard Layfield, Rainer Winter, Moris S. Eisen, Gábor Papp, Shuang Xiao, Axel Klein and Hicham Idriss

Received: 16 September 2023

Revised: 16 October 2023

Accepted: 24 October 2023

Published: 26 October 2023



Copyright: © 2023 by the authors. Licensee MDPI, Basel, Switzerland. This article is an open access article distributed under the terms and conditions of the Creative Commons Attribution (CC BY) license (<https://creativecommons.org/licenses/by/4.0/>).

1. Introduction

Electrochemical water splitting coupled with renewable energy sources is one of the most efficient and promising methods for green hydrogen production [1–3], which could tackle both the energy crisis and environmental pollution problems. The anode half reaction of water splitting is an oxygen evolution reaction (OER), which is very energy consuming, limits hydrogen production efficiency and determines the cost of hydrogen production via water splitting. So, developing efficient OER catalysts without noble metals has attracted much attention. Till now, many advanced noble-metal-free electrocatalysts have been successfully fabricated, such as transition metal (TM) oxides [4–9], hydroxide [10–13], oxyhydroxides [14,15], phosphides [16–18], etc., which presented excellent activity and stability for OER in different conditions. What’s more, the rational designed hybrids with two functional materials have also been constructed that exhibited even better performance or multifunctional properties when compared with their single counterparts [9,19,20].

Emerging as a new class of advanced materials, organic–inorganic hybrid materials (OIHs, [21]) have abundant nanoscale interfaces and redox properties, arising from strong interactions between the inorganic compounds that are rich in transition metal active sites and organic compounds that offer flexible and assembly properties. Therefore, the OIHs often exhibit various nanoscale architectures with various functionalities, leading to promising applications in many research areas such as energy storage [22–24], sensors [25–27], and catalysis [28–30], etc. Herein, we will review the recently reported OIHs and their applications in hydrogen production via water oxidation, with an emphasis on the roles of organic molecules on tuning the coordination environments of transition metal active centers. After a brief introduction of OER mechanisms, the progresses on fabrication, modification and application of MOFs and their derivatives, COF-based hybrids, as well as other rational designed and fabricated OIHs

will be fully presented and discussed (Figure 1). Finally, the perspectives, challenges and future research directions of OIHs for water oxidation will be provided.

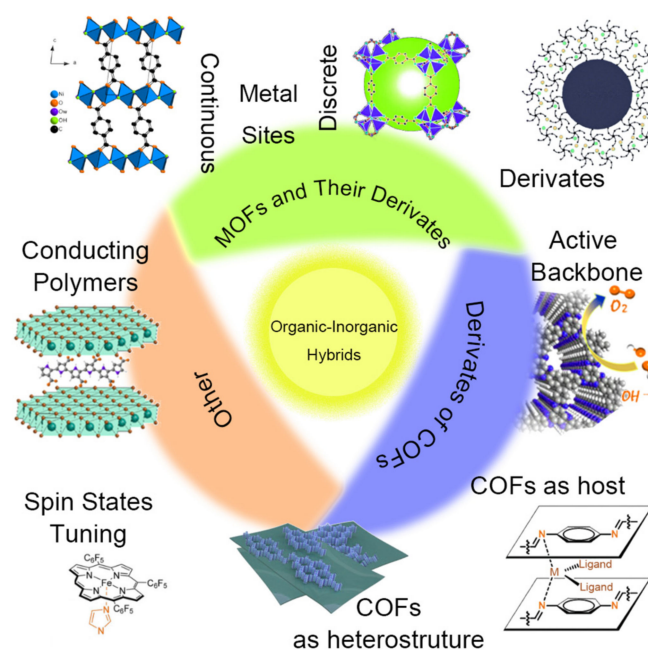


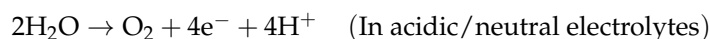
Figure 1. Typical classifications of different OIHs and the roles of organic compounds.

2. Fundamental Principles of Water Oxidation

In general, full water splitting is composed of two half reactions, the cathode hydrogen evolution reaction (HER) and the anode oxygen evolution reaction (OER). Since the OER is a four-electron oxidation process that involves four-electron transfer and an O=O bond formation, while it is a two-electron transfer process for HER, the OER on the anode is considered to be [31] the performance-limiting half reaction of the overall water splitting that limits the hydrogen production efficiency. So, in this review, we would just focus on the introduction of fundamental principles of anode OER.

2.1. Mechanisms of Electrochemical Water Oxidation

Different to the HER that has been fully investigated and the reaction mechanism has been well developed as Volmer–Heyrovsky or Volmer–Tafel processes [32–34], the OER with an equilibrium potential of 1.23 V (vs. RHE: reversible hydrogen electrode) is much more complicated [10,35–37]. The overall OER reaction in neutral/acidic and alkaline electrolytes would be written as follows:



Even though the mechanism of OER has not been settled yet, many possible reaction pathways have been proposed depending on the catalysts and reaction conditions. Herein, the most recognized OER mechanisms—the adsorbates evolution mechanism (AEM) and lattice-oxygen participated mechanism (LOM)—will be introduced and discussed in detail.

Taking OER in alkaline electrolyte for example, the four-proton-coupled electron transfer process of OER is illustrated in Figure 2a. Initially, OH^- is chemisorbed on a coordinatively unsaturated metal site and then deprotonates via a proton-coupled electron transfer process to generate $^*\text{O}$ species. Afterwards, an $^*\text{OOH}$ intermediate is formed through nucleophilic attack of OH^- , where the O–O coupling occurs. Along with the second deprotonation, the adsorbed O_2 molecule forms on the catalytic site. Finally, the adsorbed

O_2 molecule departs from the catalyst surface and the catalytic reaction cycle ends, leaving the active site to be ready for absorbing another OH^- . This AEM mechanism works well for understanding the intrinsic activities of catalysts with different chemical compositions and structures, by comparing the adsorption ability of active sites with oxygen intermediates (i.e., $*OH$, $*O$, and $*OOH$) [33,38]. However, the scaling relationship between the absorption energies of intermediates (mainly $*OH$ and $*OOH$) indicates there would be a large energy barrier for water oxidation through this reaction pathway [39–42], which is inconsistent with the advanced catalytic performance of recently developed OER catalysts such as TM oxides, hydroxides, oxyhydroxides, etc. where low overpotentials were required for efficient water splitting. What's more, the AEM mechanism proposed the catalyst surface to be a stable platform with only valence state changes during the OER process, which is contradictory to the recently observed surface reconstruction phenomenon and the pH-dependent OER activity of many catalytic materials [14,35,43,44]. Therefore, another OER mechanism named lattice oxygen participated mechanism (LOM) was proposed in order to give better scientific explanations of catalyzed OER (Figure 2b) [35,37,45].

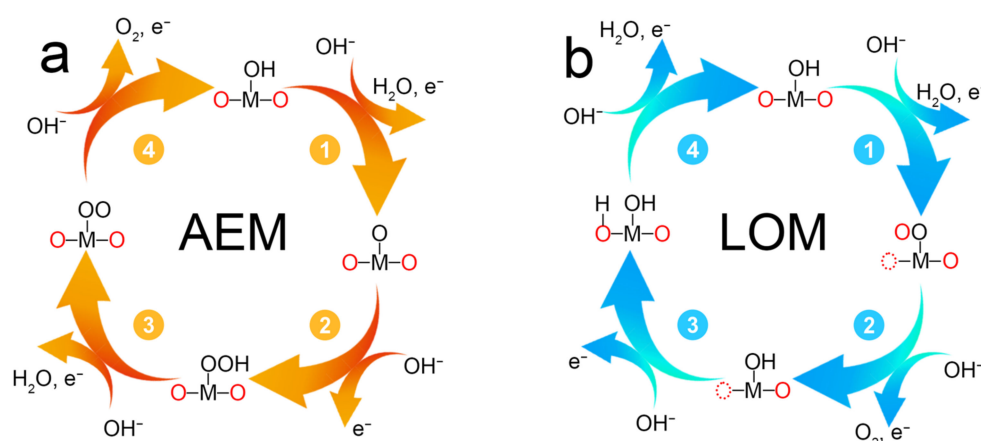


Figure 2. The reaction pathways (a) AEM and (b) LOM of water oxidation in alkaline electrolyte.

Taking OER in alkaline solution for an example again, in LOM, the OH^- is first chemisorbed on an active site, similar to the first step of an AEM mechanism. Then the formed $*OH$ species will transfer to the nearby lattice oxygen in the catalyst to generate the $*OO$ intermediate by adding another OH^- , and an oxygen vacancy near the active site will be left at the same time. Then just like the last step of AEM, the $*OO$ species will release an O_2 molecule, leaving the active site to be O-deficient. At the third step, an OH^- from the electrolyte will fill the oxygen vacancy to generate the chemisorbed OH^- . Finally, the adsorbed OH^- will lose a proton by reacting with OH^- in the electrolyte and the active site will be recovered to initiate the next reaction cycle. Therefore, OER following the LOM mechanism usually shows pH-dependent activity due to the non-concerted nature of electron–proton transfer in the second and third steps [46]. However, due to the involvement of lattice oxygen in the catalytic reaction, the surface layer of catalysts may undergo a reconstruction process, which deactivates the catalysts [47].

In general, the mechanism of OER depends on the intrinsic properties of the M–O bond that is related to the physicochemical property such as the band structure of catalysts. The two OER mechanisms discussed above could explain different experimental observations but could not cover all issues discovered in OER processes, due to the complexity of catalytic materials. So, it is critically important to identify the structure and coordination environments of active sites, especially the dynamic change in structure of the catalytic sites under OER conditions. However, the fast reaction rate that occurs on the micro- to milli-second scale on particular reaction sites at atomic levels, makes it a great challenge to obtain real-time information of the OER. Developing in situ/operando techniques with high

spatiotemporal resolution would be a promising way to visualize the dynamic behavior of active sites and shed light on the revelation of OER mechanisms.

2.2. Important Descriptors for the Evaluation of Electrochemical Performance

In this section, we will introduce some descriptors such as overpotential, Tafel slope, electrochemical double-layer capacitance, stability and Faradaic efficiency that are critical for evaluating the electrochemical water oxidation performance of the organic–inorganic hybrid materials.

The first important descriptor is the overpotential (η), which is a quantification of the part of the operating potential that exceeds the equilibrium potential. It represents the excess potential required to overcome the intrinsic kinetic barriers in an electrochemical reaction. In general, an overpotential is identified through the polarization curve (after internal resistance compensation). Typically, researchers compare overpotentials at a specific current density (such as 10 mA cm^{-2}) as it provides a standardized metric for evaluating the performance of different electrocatalytic materials or systems. The smaller the overpotential, the higher the electrocatalytic activity.

The second important descriptor, Tafel slope (b), is the slope of the linear region in a Tafel plot obtained by transferring the uncompensated polarization curve into a logarithmic value with base 10 on the current density. This linear region is fitted using the Tafel equation:

$$\eta = a + b \log_{10} j \quad (\text{Tafel equation})$$

where η and j stand for the overpotential and current density, respectively, and a and b are the intercept and slope obtained from the fitted curve. In other words, the Tafel slope describes the additional potential that needs to be applied for every 10-fold increase in current density over a certain range, reflecting the kinetic nature of the reaction.

The third descriptor frequently mentioned in the literature is the electrochemical double-layer capacitance (C_{dl}). The electrochemical double-layer capacitance reflects the electrochemical surface area of the actual contact interface between the electrode and the electrolyte [48,49]. In the case of the OIHs discussed in this review, the porous structures of these materials lead to high contact areas, which can be characterized by measuring the C_{dl} .

For practical applications, stability is a crucial parameter reflecting the ability of an electrocatalyst to maintain its activity over extended periods. Typically, it is described by the number of cycles of cyclic voltametric (CV) measurements that maintain the polarization curves nearly unchanged. The shift of the redox peaks between different cycles can reveal changes in the electrochemical properties of the catalyst or changes in the catalysts themselves, which may be crucial for the studies investigating the electrochemical water oxidation performances of OIHs. However, the stability determined by this method depends on the operating conditions such as scanning rates and potential intervals, so it is inconvenient for researchers to compare the stability of their catalyst with others. Thus, many researchers also conduct chronoamperometry or chronopotentiometry measurements on a specific current density (e.g., 10 mA cm^{-2}) or potential to illustrate how the current density or potential varies with time, providing insights into the stability of the catalyst [50].

Faradaic efficiency (FE) is another critical descriptor to determine the current density from water oxidation, rather than undesirable but unavoidable side reactions such as the oxidation of organic components in OIHs. Generally, the organic molecules, such as carboxylic acids, would be oxidized during the high potential (1.36 V vs. RHE [51]). So, it is necessary to quantify the portion of the current from the OER [52]. This quantification enables the determination of FE that represents the effectiveness of the electrochemical process in converting water into oxygen. For an electrochemical reaction involving z electrons, the transferred charge Q can be calculated according to the Faradaic laws of electrolysis below,

$$Q = nzF \quad (\text{Faradaic equation})$$

where the n and F stand for the amount of substance involved in the reaction and the Faradaic constant. As a result, the accuracy of FE is based on the precise measurement of produced oxygen during the testing time. Generally, the most widely used method to quantify the O_2 yield is the application of a gas chromatogram with a thermal conductivity detector. The FE determined by this method is most accurate. However, GC equipment should be settled and coupled with an electrochemical workstation. Another frequently used method is based on a rotating ring-disk electrode setup, in which the catalyst is loaded on the disk that acts as the first working electrode and delivers a constant current to generate oxygen. A relatively low potential (typically 0.4 V vs. RHE) is set on the ring that works as the second working electrode, where the generated oxygen is reduced. However, not all the oxygen generated on the disk could be timely reduced on the ring, leading to an underestimated FE. Therefore, the oxygen collection coefficient could be first ascertained by using IrO_2 as a catalyst. What's more, the Archimedes drainage method was also applied in many studies to assess the yield of produced O_2 . However, the FE would be overestimated if there were any other gas products in addition to oxygen. So, attention should be paid to the determination methods when comparing the FE of water oxidation catalyzed by IOHs.

3. Organic–Inorganic Hybrid Materials for Electrochemical Water Oxidation

For most cases, the electrochemical activity of OIHs is still provided by metal sites, but the coordination environments of the metal sites that are greatly influenced by the ligands have been found to play critical roles on the catalytic performance of the materials. In this section, we would review different kinds of OIHs and their derivatives, as well as the effects of organic components in modulating the coordination environment of catalytic sites and then improving their performance towards water oxidation.

3.1. Metal–Organic Frameworks (MOFs) and Their Derivates

In 1995, Prof. Yaghi [53] synthesized a crystalline material consisting of coordination bonds between transitional metal cation Co^{2+} and multidentate organic linker benzenedicarboxylic acid (BTC) for the first time and named this type of material a metal–organic framework (MOF) material. Since then, many different types of MOFs such as iso-reticular MOFs [54], zeolitic imidazolate frameworks (ZIFs) [55], Matériel Institut Lavoisier [56], etc. have been successfully synthesized. Recently, MOFs have been widely studied for applications in various fields such as gas separation [57–60], water purification [61,62], industrial catalysis [62–66], drug delivery [67], etc. due to their structural merits including high specific surface area, high porosity, and designable micromorphology. Particularly, MOFs are considered to have the advantages of both homogeneous and heterogeneous catalysts for electrochemical water splitting [68], due to the highly porous nature of the MOFs that are perfect for immobilizing active metal complexes. In this section, we will discuss the progress of MOFs and their derivatives towards electrochemical water oxidation as summarized in Table 1.

Table 1. Summary of data for MOFs and their derivatives used as water oxidation catalysts.

Catalyst	Electrode Substrate	Electrolyte	Overpotential (V, at 10 mA cm ⁻²)	Stability	Double-Layer Capacitance (mF cm ⁻²)	Faradaic Efficiency (%)	Reference
NiCo-UMOFNs	GC ¹	1.0 M KOH	0.250	40,000 s	/	99.3	[69]
2D MOF-Fe/Co(1:2)	GC disks	1.0 M KOH	0.238	50,000 s	66.9	/	[70]
NiFe-NFF	NFF ²	1.0 M KOH	0.227	1000 cycles	12.72	100	[71]
Co ₃ Fe-MOF	GC	1.0 M KOH	0.280	10 h	17.74	/	[72]
Fe ₂ Ni-MOF	NF ³	1.0 M KOH	0.213	1033 h ⁴	5.8	/	[73]
Ni _{0.9} Fe _{0.1} -MOF-74	GC	1.0 M KOH	0.198	/	/	99.6	[74]
Fe ₂ Ni-BPTC (NNU-23)	CC ⁵	0.1 M KOH	0.365	2000 cycles	5.10	/	[75]
CTGU-10c2	GC	0.1 M KOH	0.280	1000 cycles	8.9	/	[76]
Ni@N-HCGHF	GC	1.0 M KOH	0.260	2000 cycles	/	/	[77]
MPN@Fe ₃ O ₄	GC	1.0 M KOH	0.260	24 h	25.8	/	[78]
NiCo _{2-x} Fe _x O ₄ NBs	CP ⁶	1.0 M KOH	0.274	25 h	30.7	/	[79]

¹ GC stands for glass carbon; ² NFF stands for nickel iron foam; ³ NF stands for nickel foam; ⁴ 1033 h at 100 mA cm⁻² followed by another 200 h at 500 mA cm⁻²; ⁵ CC stands for carbon cloth; and ⁶ CP stands for carbon paper.

Mesbah et al. [80,81] designed and synthesized a MOF with an infinite chain of nickel octahedra similar to that in metal hydroxides, in which the metal ions were linked together via O and H atoms (Figure 3a). Considering that transition metal hydroxides were efficient catalysts for electrochemical water oxidation, many studies have been conducted to investigate and modulate the OER performance of this kind of MOF [69–72]. By using benzenedicarboxylic acid (BDC) as the organic ligands, Zhao et al. [69] fabricated ultrathin NiCo bimetal–organic framework nanosheets, which showed advanced alkaline OER activity with small overpotentials of 0.250 V and 0.189 V at 10 mA cm⁻² when loading on glass carbon and copper foam, respectively. According to atomic force microscopy (AFM, Figure 3d), they found the thickness of as-prepared NiCo MOF nanosheets was only ca. 3.1 nm, suggesting a crystal structure of 2D bimetal layers that were separated by BDC molecules (Figure 3c). By combining the ex situ extended X-ray absorption fine structure (EXAFS) data with ab initio calculations (Figure 3b), they confirmed the existence of abundant coordinatively unsaturated metal sites on the ultrathin NiCo-MOFs, which were determined to be the dominating active sites. Then, FeCo bimetallic MOFs with different morphologies were also reported by using BDC as the organic linker [70]. The authors investigated the effects of transition metal ratio and found that the one with Fe/Co~1:2 exhibited the best OER performance, with a low overpotential of 0.238 V at 10 mA cm⁻² and a small Tafel slope of 52 mV dec⁻¹ in alkaline solution. However, both the chemical stability of the formed NiFe MOFs were undesirable, which showed a clear degradation after 30 days maintained in the air in the form of slurry. Similarly, Ni(Fe)-MOFs with an ultrathin nanosheet (ca. 1.56 nm) microstructure (Figure 3e) were fabricated by using NiFe foam as a semi-sacrificial template [71]. The strong coupling effects between the Ni and Fe sites were observed, leading to an advanced OER activity and relatively improved stability in 1.0 M KOH with a FE of nearly 100%. However, the FE in this study was measured by the above-mentioned Archimedes drainage method, which was actually overestimated if there were any other gas byproducts such as CO or CO₂ generated by the oxidation of organic components in the MOFs. Furthermore, the stability of 15 h at 20 mA cm⁻² was actually not enough for practical applications.

To investigate the reason behind the poor stability of MOFs, Li et al. [72] carefully characterized the structure of CoFe-MOF nanosheets before and after the OER catalysis. Based on the high-resolution transmission electron microscopy (HRTEM) images, they observed a lattice fringe of 0.247 nm with 60° that could be ascribed to the (010) and (100) plane of Co(Fe)OOH (Figure 3f), suggesting the transformation of CoFe-MOFs to the corresponding oxyhydroxides during the OER process. The transformation of MOFs to the other phases would inevitably lead to structure collapse and deteriorate their stability [82]. However, the formed metal hydroxides/oxyhydroxides were found to be the real active sites for OER electrochemical catalysis. So, obtaining comprehensive knowledge on the transformation processes of transition metal sites during the OER process is critical for

revealing the reaction mechanism and shedding light on the design of novel catalytic materials, which leads to more extensive studies by coupling ex situ and in situ characterization techniques [73,74].

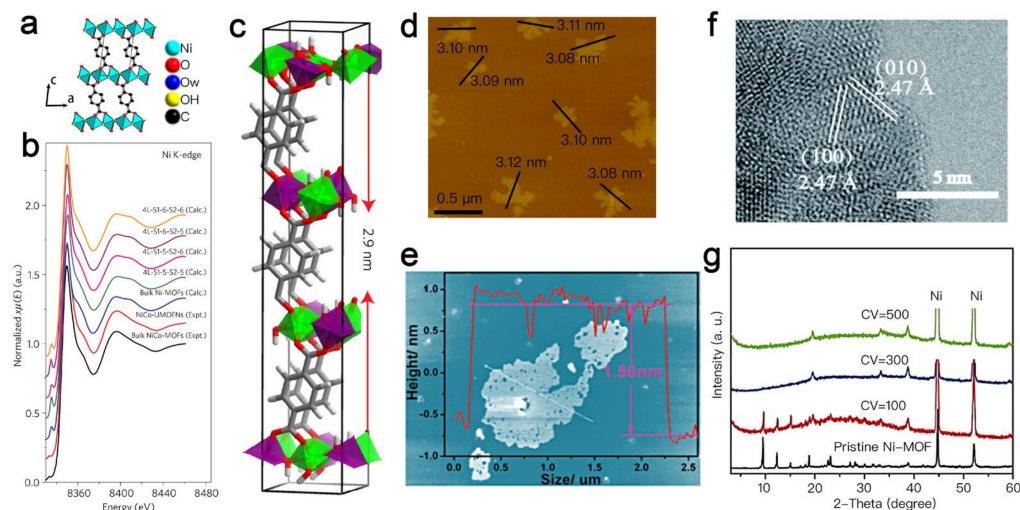


Figure 3. (a) MOF structure synthesized by Mesbah et al. [80], viewed down the *b* axes. Copyright © 2014, American Chemical Society. (b) Comparison of the Ni K-edge XANES experimental and theoretical spectra including NiCo-UMOFNs, bulk NiCo-MOFs and the theoretical structural models with unsaturated metal sites. (c) Theoretical thickness of NiCo-UMOFNs with four metal coordination layers. (d) AFM image of NiCo-UMOFNs prepared by Zhao et al. [69] showing measured dimensions of individual flakes. Copyright © 2016, Springer Nature Limited. (e) AFM image of NiFe-NFF synthesized by Cao et al. [71]. Copyright © 2018, WILEY-VCH Verlag GmbH & Co. KGaA, Weinheim, Germany. (f) TEM images of OER activated Co₃Fe-MOF synthesized by Li et al. [72]. Copyright © 2020, The Royal Society of Chemistry. (g) XRD patterns of Ni-MOF nanoarrays after different CV tests, which were synthesized by Wang et al. [73]. Copyright © 2021, American Chemical Society.

Wang et al. [73] investigated the effect of Fe in the bimetallic MOF (named NiFe-MOF) with 2D nanobelt microstructure through ex situ XRD characterizations. The NiFe-MOFs were vertically grown on the nickel foam and exhibited a greatly increased OER activity after 100 cycles of CV scanning in 1 M KOH electrolyte. A similar phenomenon was also observed in a single-metal Fe-MOF, but the Ni-MOF showed negligible change. The authors found that the characteristic diffraction peaks of the NiFe-MOF and Fe-MOF in ex situ XRD spectra were retained after 500 CV cycles, but those of the Ni-MOF disappeared at 300 cycles, suggesting the good stability of MOFs with the existence of Fe (Figure 3g). What's more, the ratio of Fe³⁺/Fe²⁺ increased from 2/5 to 8.9/5 from the 10th to the 100th CV cycle in the FeNi-MOF, indicating the dependence of enhanced OER performance with the formation of high-valence Fe³⁺ species, which could in turn strengthen the electrostatic interaction between the metal nodes and organic ligand and then contribute to the stability of the bimetal MOFs. Noting that this electrode worked at 100 mA cm⁻² for more than 1033 h without obvious degradation, suggests a much better stability than the other MOF materials. Taking advantages of in situ synchrotron X-ray absorption spectroscopy (XAS) that could provide the time-resolved information on local bonding of specific elements, Zhao et al. [74] tracked the self-reconstruction of bimetal MOF-74 under OER conditions. Firstly, they found that the Ni valence increases to +3, and the Co valence was nearly unchanged at the 1.3 V vs. RHE, while both increased at a higher potential (Figure 4a). By fitting the result of XAS, they also found that both the bond length and coordination number of Ni-O and Ni-metal decreased significantly at the applied potential of E = 1.3 V vs. RHE (Figure 4b), due to the formation of Ni(OH)₂ and NiOOH (Figure 4c). They also synthesized MOFs with different chemical compositions and found that only with the existence of a Co element in the MOFs, would the bond length and coordination number

of Ni-O and Ni-metal decrease dramatically, while those of Co-O and Co-metal showed a similar decreasing pattern even in the MOFs without Ni elements (Figure 4d). Based on these results, they proposed that the existence of Co species in the MOFs was crucial for the formation of Ni(Co)OOH which was the real active site for alkaline OER.

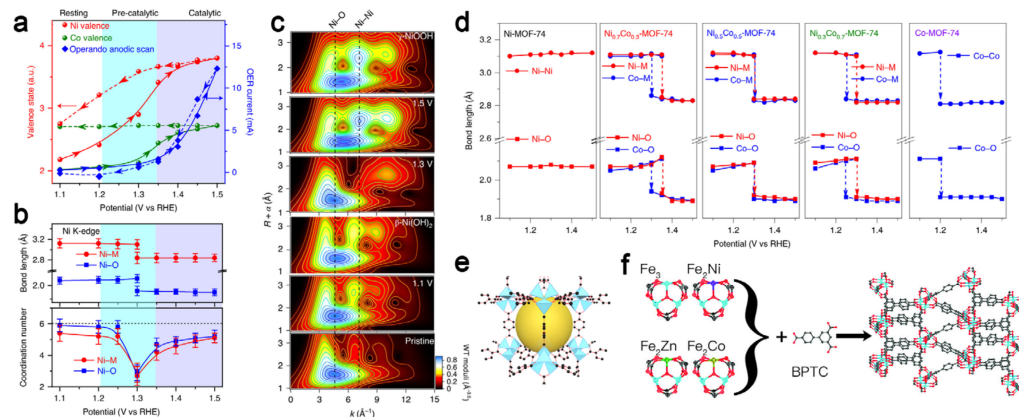


Figure 4. (a) Change in the Ni and Co valence states and OER current as a function of applied potentials. (b) Changes in bond length and coordination number for the Ni–O and Ni–M coordination shells. (c) Comparison of Ni K-edge EXAFS wavelet transforms recorded for the standard references, and the bimetal MOF-74 in different conditions. (d) Change in bond length as a function of applied potentials for Ni_{1-x}Co_x-MOF-74. Copyright © 2020, the Author(s), under exclusive license to Springer Nature Limited. (e) The structure of MOF-5 synthesized by Yaghi’s group [83]. (f) The 3D framework of NNU-21–24 connected by trinuclear metal clusters and biphenyl-3,4’,5-tricarboxylic acid (BPTC) ligands prepared by Wang et al. [75].

In addition to the above-mentioned MOFs with continuous metal sites, the MOFs with isolated metal clusters and a large cavity in the structure were also intensively investigated [75,76]. Most of these MOFs are descendants of MOF-5 synthesized by Yaghi’s group [83] in 1999, with metal carboxylate clusters as the metal center (Figure 4e). Wang et al. [75] synthesized a MOFs with NiFe clusters by replacing the CH₃COO[−] groups in the Fe₂M(μ₃-O)(CH₃COO)₆(H₂O)₃ (M=Fe, Co, Ni, Zn) clusters with biphenyl-3,4’,5-tricarboxylic acid (BPTC) ligands (Figure 4f). Although scanning electron microscopy (SEM) images showed the size of the particles they synthesized to be almost 200 μm, they showed advanced OER performances even when loaded on glassy carbon electrodes due to abundant nanopores in the structure. Then, this type of MOF with three-metal clusters and tunable chemical compositions (Co₃, Co₂Ni, CoNi₂, and Ni₃) was reported by Zhou et al. [76]. Depending on the Co/Ni ratio, the morphology of these MOFs showed nanosphere or nanobelt microstructures assembled by nanosheets as the building block. Among them, the CoNi₂-MOF exhibited the best OER activity with an overpotential of 0.28 V at 10 mA cm^{−2}, and a Tafel slope of 58 mV dec^{−1} in 0.1 M KOH, which was attributed to the coupling effects between Ni and Co, as well as the ultrathin microstructure with the thickness of ca. 1.1 nm.

Apart from the direct application of MOFs as electrocatalysts, their derivatives obtained by controlled post-processing treatments have been attracting widespread attention due to the much-increased stability under OER conditions. A commonly used strategy to fabricate MOF derivatives is pyrolysis. In 2020, Yan et al. [77] found that pyrolysis of Ni-based MOFs with BTC as a ligand resulted in the synthesis of composites of Ni nanoparticles and carbon nanotubes (CNTs), respectively. By pyrolyzing the mixture of Ni-based MOF and graphene oxide (GO), they synthesized a freestanding 3D hetero-structured film composed of Ni nanoparticles and 1D CNT, which were linked with the 2D rGO nanosheets to stitch the 3D freestanding film (Figure 5a). The as-prepared hetero-structured freestanding film could be easily transferred onto the surface of conductive substrate without any binding, which could serve as a working electrode. After electrochemical evaluation, they found that

the prepared freestanding film named Ni@N-HCGHF exhibited excellent electrocatalytic activity for both OER and HER due to the synergistic effect of the N-doped carbon shell and Ni nanoparticles in the films. The electrolyzer assembled only using this electrode worked at 1.6 V for more than 20 h without obvious degradation, suggesting good stability.

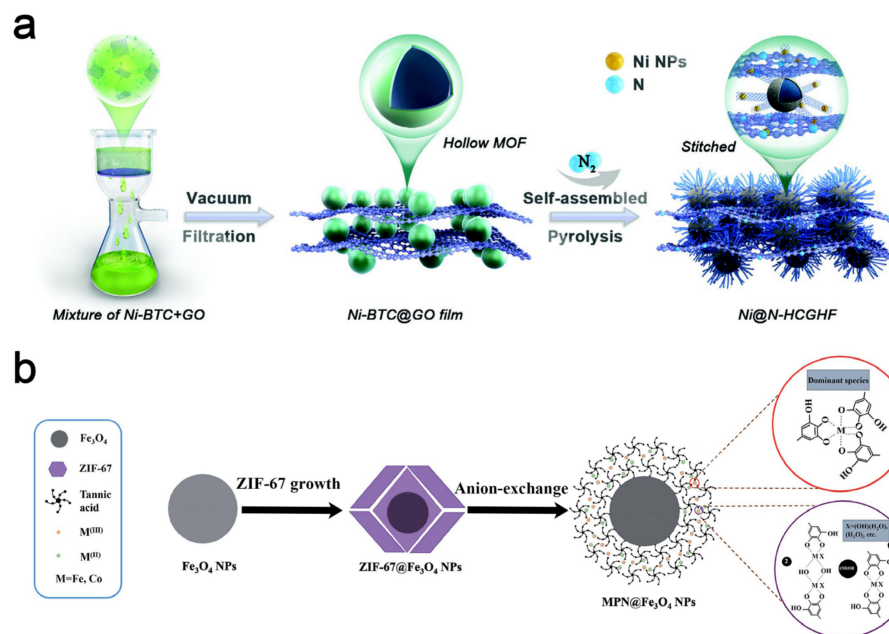


Figure 5. (a) Schematic of the preparation process of Ni@N-HCGHF by Yan et al. [77]. Copyright © 2020, Wiley-VCH GmbH. (b) Schematic illustration of the formation of organic-inorganic Co/Fe-polyphenolic networks@Fe₃O₄ hybrid nanostructures by Jia et al. [78]. Copyright © 2019, The Royal Society of Chemistry.

Noticing that organic ligands will greatly influence the mass transport and utilization of active sites, rational tuning of the nature of organic ligands in MOFs would be an ideal approach to enhance their catalytic performance. Recently, Jia et al. [78] synthesized a dodecahedral shaped core-shell structured catalyst of ZIF-67@Fe₃O₄ and then dispersed it in tannic acid (TA) methanol solution to convert the shell to a layer of amorphous metal-polyphenolic networks (MPNs), leading to the formation of a catalyst named MPN@Fe₃O₄ with a changed organic linker (Figure 5b). Compared to the original Fe₃O₄ nanoparticles, they found that the specific surface area of ZIF-67@Fe₃O₄ was greatly increased from 20.5 m² g⁻¹ to 746.1 m² g⁻¹, while it decreased to 8.71 m² g⁻¹ with the conversion of the ZIF-67 shell to the amorphous MPNs. However, MPN@Fe₃O₄ exhibited better OER performance (η_{10} = ca. 0.26 V) and higher double-layer capacitance (C_{dl} , 25.8 mF cm⁻²) than that of Fe₃O₄ (ca. 0.453 V, 2.26 mF cm⁻²) and ZIF-67@Fe₃O₄ (0.335 V, 6.11 mF cm⁻²). The authors proposed that the amorphous MPN shell could lead to an increased density of electrochemically active sites, which was further confirmed by the results observed in the FeMPN@Fe₃O₄ and CoMPN@ZIF-67 systems they designed. Also, by etching ZIF-76 with TA, Huang et al. [79] synthesized TA-Co nanoboxes (TA-Co NBs) and conducted a cation exchange reaction to obtain trimetallic TA-NiCo_{2-x}Fe_xO₄ NBs, which were further calcinated in air and converted to spinel NiCo_{2-x}Fe_xO₄ NBs. Though the as-prepared NiCo_{2-x}Fe_xO₄ NBs presented good OER performance with a low overpotential of 0.274 V at 10 mA cm⁻² for more than 25 h, it actually converted from the spinel oxide to the corresponding oxyhydroxides during the OER processes via surface reconstruction, suggesting the importance of rational selection of organic ligands and post-treatment condition for preparing highly active and stable MOF derivatives towards efficient OER.

In summary, various types of MOFs and techniques for synthesizing ultra-thin MOFs have been developed. However, their stability remains an unresolved challenge. Out of the

mentioned MOF materials, only the Fe₂Ni-MOF prepared by Wang et al. [73] demonstrated the necessary stability for industrial applications. However, during the 1033 h chronopotentiometry measurement, the crystal structure of the MOF collapsed and slowly converted to an amorphous structure. But because of the lack of Faradaic efficiency data and detailed characterizations of the catalyst after long-term OER, it became uncertain whether the organic components were oxidized or still existed in the final catalytic material. So, it is suggested here that to better assess the OER performance and understand the catalytic mechanism, the Faradaic efficiency as well as the conversion processes should be paid more attention to in future studies by using OIHs as OER catalysts.

Regarding the synthetic routes of MOF derivatives, the existing synthetic methods are limited to pyrolysis and ion-exchange methods, which still show limitations in terms of achieving sufficient OER activity and stability. More methods should be explored in future studies that allow for better control over the composition, structure, and morphology of MOF derivatives. This would be involved in the development of novel precursors, template-assisted synthesis methods, or post-synthetic modifications to tailor the properties of the materials specifically for OER applications.

3.2. Derivates of Covalent Organic Frameworks (COFs)

Covalent organic frameworks (COFs), which were first synthesized by Yaghi's group in 2005 [84], have similar structural properties to that of MOFs, such as high porosity, tunable structure, etc., that would benefit the catalytic processes. However, unlike MOFs, which are coordinately linked by metal ions and organic ligands, COFs are composed of non-metal elements that connected by covalent bonds (Figure 6, [85]). The applications of COFs and their derivates in electrocatalysis could be generally divided as the COF-based hybrids [86–95] and the pristine COFs with active backbones [96,97]. In this section, we will discuss the recently reported COF-based OIHs for water oxidation, as presented in Table 2. Furthermore, we will delve into the specific techniques used for modifying the active centers, with illustrative examples.

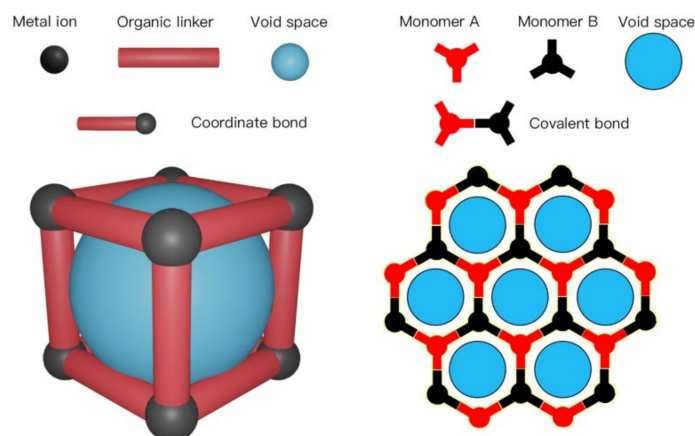


Figure 6. A schematic representation of the MOF (left) and COF (right) structures.

Table 2. Summary of data for COFs and their derivates used as a water oxidation catalyst.

Catalyst	Substrate	Electrolyte	Overpotential (V, at 10 mA cm ⁻²)	Stability	Double-Layer Capacitance (mF cm ⁻²)	Faradaic Efficiency (%)	Reference
Co ₄ Ni ₁₂ -COF	GC	0.1 M KOH	0.258	13 h	0.398	90.0	[87]
Ni ₃ N-COF	GC	1.0 M KOH	0.230	20 h	3.63 × 10 ⁻²	98.0 ¹	[88]
COF-C ₄ N	CC	1.0 M KOH	0.349	20 h	5.01	/	[97]
N-MoS ₂ @COF-C ₄ N1:1	CC	1.0 M KOH	0.349	70,000 s	4.19	/	[90]
Co@COF-C ₄ N1:1	CC	1.0 M KOH	0.280	20 h	42.04	/	[91]
CoV@COF-SO ₃	/	1.0 M KOH	0.318	1000 cycles	3.38	99.0	[92]
(cyclen@NiFe)@COF-SO ₃	CP	1.0 M KOH	0.276	25 h	0.462	99.0	[93]
Nb ₂ CO ₂ @COF	GC	1.0 M KOH	0.373	10 h	2.17	/	[94]

¹ 98% at 1 mA cm⁻², while reduced to 58% at 10 mA cm⁻².

Early in 2011, Wang's group [86] synthesized a COF with microporous channels (ca. 1.8 nm) for the first time (named COF-LZU1) and used it as a host to introduce palladium as the active species in the interlayer to catalyze the Suzuki–Miyaura coupling reaction. With this idea of using COF as a host, Vaidhyathan's group grew $\text{Co}_x\text{Ni}_y(\text{OH})_2$ and Ni_3N nanoparticles on a flexible COF and used them for electrochemical water oxidation for the first time [87,88]. The prepared $\text{Co}_4\text{Ni}_{12}$ -COF shows excellent OER performance, requiring overpotentials of only 0.258 V at 10 mA cm^{-2} in 0.1 M KOH. By HRTEM, they confirmed that the nanoparticles resided within the COF rather than lying on the surface to form a heterostructure. More specifically, they hypothesized that the nanoparticles could be sandwiched between the two sp^3 nitrogen atoms of the COF based on theoretical calculations. Delivering a stable current at 1.5 V vs. RHE for 13 h, the catalyst showed an acceptable stability but far from industrial applications. The Ni_3N -COF reported in the same year also exhibited superior OER performance, with a small overpotential of 0.230 V at 10 mA cm^{-2} and was stable at this current density over 20 h in 1.0 M KOH. Rather than directly growing nanoparticles within the COF, Luo's group used interlayer coordination to introduce metal sites in the COF [92,93]. They first synthesized a COF with a sulfonic acid group (named as COF- SO_3H) via a condensation reaction by using both the 2,5-diaminobenzenesulfonic and 2,4,6-triformylphloroglucinol as the precursor. Subsequently, the COF- SO_3H was aminated in concentrated ammonia and the NH_4 @COF- SO_3 with NH_4^+ ions in the pores was formed. Then, a cation exchange process was conducted to replace the ammonium ions therein by catalytically active metal ions (i.e., Co^{2+} and V^{3+}) or metal complexes (i.e., cyclen@NiFe complex), and finally, the CoV@COF- SO_3 and (cyclen@NiFe)@COF- SO_3 (Figure 7a) with different molar ratio of metals were obtained. When used to catalyze OER, the CoV@COF- SO_3 performed much worse than (cyclen@NiFe)@COF- SO_3 , which had organic components. According to XPS spectra, the Ni-N and Fe-N bonds in the organic–inorganic hybrid of (cyclen@NiFe)@COF- SO_3 were found to be immobilized through the coordination of the metal ions to N in the cyclen. Though the incorporation of the bimetal cyclen@NiFe complex into the pore channel of NH_4 @COF- SO_3 decreased the specific surface area from 110 to $42 \text{ m}^2 \text{ g}^{-1}$, the catalytic activity of the hybrid was still far beyond that of the two single component counterparts (Figure 7b). Based on various experimental characterizations, the advanced activity of (cyclen@NiFe)@COF- SO_3 hybrid was proposed to arise from the significant bimetallic electronic interactions between and transition metals Ni and Fe, even though they were separated by the organic linkers. In addition to the application of COFs as the substrates to synthesize OIHs, COFs were also designed to directly grow on the surface of inorganic materials, such as the hetero-structured Nb_2CO_2 @COF (Figure 7c) made by Zong et al. [94]. The as-prepared Nb_2CO_2 @COF hybrids delicately overcame the disadvantage of easy aggregation of Nb_2CO_2 MXene, and hence exposed more active sites. Moreover, the confinement effects of COF were found to affect the distribution of oxygen molecules on the surface of the catalyst and promoted the orderly and efficient reactions, further contributing to the improved stability of the hybrids for OER and making it efficient in rechargeable zinc-air batteries.

Later in 2019, Zhang's group found a COF- C_4N that would have an OER active backbone based on theoretical calculations [97]. According to this finding, they further synthesized the COF- C_4N and confirmed its excellent OER performance with an overpotential of 0.349 V at 10 mA cm^{-2} and a Tafel slope of 34 mV dec^{-1} in 1.0 M KOH. Three years later, they further grew MoS_2 vertically on the COF- C_4N through a hydrothermal method and obtained a MoS_2 /COF- C_4N hybrid, which exhibited advanced catalytic activity for both alkaline OER and acidic HER [90], arising from the abundant OER active sites in the COF backbone and HER active centers in the well-dispersed and vertically grown MoS_2 nanosheets, respectively. What's more, the interface between the COF and MoS_2 further enhanced the charge transfer, resulting in the good bifunctional activity of the prepared MoS_2 /COF- C_4N hybrids. Then, by impregnating the COF- C_4N in an $\text{M}(\text{OAc})_2$ ($\text{M}=\text{Mn}$, Fe, Co, Ni, or Cu) methanol solution, the authors synthesized a series of hybrid materials

named M-COF-C₄N [91]. Among these hybrids, the Co-COF-C₄N exhibited the best OER performance, requiring only a low overpotential of 0.28 V at 10 mA cm⁻², and a Tafel slope of 69 mV dec⁻¹. The strong d-p_z coupling between transition metal Co and organic COF backbone, as well as the fast charge transfer, were found to facilitate the formation of key intermediates during the OER process and hence improved the catalyzed OER kinetics.

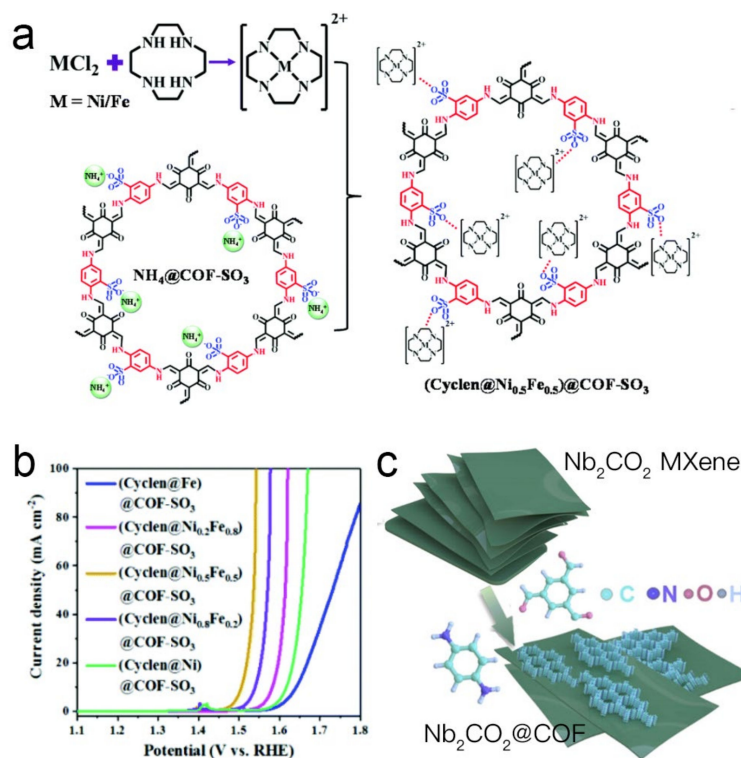


Figure 7. (a) Preparation of COF-anchored NiFe complex $(Cyclen@Ni_{0.5}Fe_{0.5})@COF-SO_3$ synthesized by Feng et al. [93]. (b) Polarization curves of their COFs-based materials. Copyright © 2020, The Royal Society of Chemistry. (c) Schematic illustration of the preparation process of $Nb_2CO_2@COF$ by Zong et al. [94]. Copyright © 2022, American Chemical Society.

To summarize, there has been extensive exploration of two approaches: one involves the insertion of metal ions/nanoparticles into the interlayers or nanochannels of COFs, while the other focuses on synthesizing COF-based heterostructures. However, simultaneously achieving precise control over the size of nanoparticles and nanochannels that could further improve the catalytic performance of the COF-based OER catalysts remains challenging and still needs extensive studies. In addition, some studies did not give data on the Faradaic efficiency of water oxidation, which should be emphasized in further research to confirm the accuracy of the reported electrochemical performance towards water oxidation.

3.3. Other Organic–Inorganic Hybrid Materials (OIHs) for Electrochemical Water Oxidation

Though MOFs and the derivatives of COFs are the most typical and widely investigated OIHs, there are also many studies on the rational coupling of organic molecules and inorganic compounds to generate functional hybrids for water oxidation that have achieved some important breakthroughs, which will be introduced and discussed in this section, as illustrated in Table 3.

Table 3. Summary of data for other OIHs used as water oxidation catalysts.

Catalyst	Substrate	Electrolyte	Overpotential (V, at 10 mA cm ⁻²)	Stability	Double-Layer Capacitance (mF cm ⁻²)	Faradaic Efficiency (%)	Reference
LDH-ppy	NF	1.0 M KOH	0.248	10 h	/	94.5	[98]
CuZrO ₃ @ppy	SSS ¹	1.0 M KOH	0.226	50 h	0.96	/	[99]
NiFe-BTC//G	graphite foil	1.0 M KOH	0.106	150 h ²	81.6	100	[100]
CoCor-CNT	GC	0.1 M pH 7 phosphate buffer	0.470	100 cycles	/	/	[101]
FePor/CNT	GC	0.1 M KOH	0.500	8 h	0.21	98.0	[102]

¹ SSS stands for stainless steel strip; ² the stability test was performed in 0.1 M KOH.

Since most of the transition metal-based catalysts such as TM oxides [103,104], hydroxides [12,105], etc. have inferior conductivity, many researches have tried to couple the catalytically active TM compounds with conductive materials to increase the charge transfer characters, and many functional hybrids such as TM LDH/CNT [106–108], TM LDH/rGO [109,110], MoS₂/rGO [111,112], etc. have been successfully developed. All of these hybrids showed a much-improved performance. In addition to the carbon materials, the conductive polymers that also have high conductivity and even outperform that of rGO, have also attracted much attention [113–118]. By taking the poly-pyrrole (ppy) that has a high conductivity of 105 S cm⁻¹ as the typical example, Ju et al. [98] coupled the OER active NiFe LDH with it and synthesized the LDH-ppy hybrid via a facile interlayer anion exchange process followed by the in situ polymerization (Figure 8a). The synthesized LDH-ppy showed a nanosheet morphology with a lateral size of 2–3 μm and a thickness of 4–40 nm, similar to the pristine LDH. Through XPS survey, they found that the direct contact of conductive ppy with active transition metal centers at the atomic level greatly enhanced the electron transfer from Ni sites to the surrounding Fe sites, leading to a larger ratio of Ni(III)/Ni(II). The much more active Ni(III) species in the LHD-ppy greatly reduced the overpotential of the alkaline OER. What's more, the authors carried out the in situ AFM-scanning electrochemical microscopy (SECM) and electrochemical quartz crystal microbalance with dissipation (EQCM-D) and tracked the OER processes on the surface of the LDH-ppy hybrids. They found that the intercalation of ppy made the LDH-ppy hybrid structure much more dynamically adaptive and robust to the OER process, indicating the positive role of organic polymer for increasing both the charge transfer and long-term stability of the catalysts. Inspired by their work, Aman et al. [99] also synthesized nanocomposites of poly-pyrrole and CuZrO₃, named CuZrO₃@ppy. They found that the introduction of the conductive polymer ppy reduced the Tafel slope from 113 mV dec⁻¹ to 76 mV dec⁻¹, which greatly improved the kinetics of OER. In 2019, Li et al. [101] immobilized Co corroles on CNT to obtain CoCor-CNT. The as-prepared CoCor-CNT exhibited a pH universal bifunctional catalytic performance for both OER and HER, which worked well in 0.5 M H₂SO₄, (pH = 1.0), 0.1 M phosphate buffer (pH = 7.0), and 1.0 M KOH (pH = 14.0). Based on a series of experiments, the authors found that the chemical properties of amino groups were crucial for catalytic activity of the formed hybrid materials. Some researchers have taken an alternative approach, as demonstrated by the work by Lyu et al. [100], where they incorporated poorly conducting MOF materials into highly conducting graphene to synthesize NiFe-BTC//G with extremely high activity. The prepared NiFe-BTC//G only required an overpotential of 0.106 V at 10 mA cm⁻², significantly lower than that of the bulk NiFe-BTC without graphene (0.399 V).

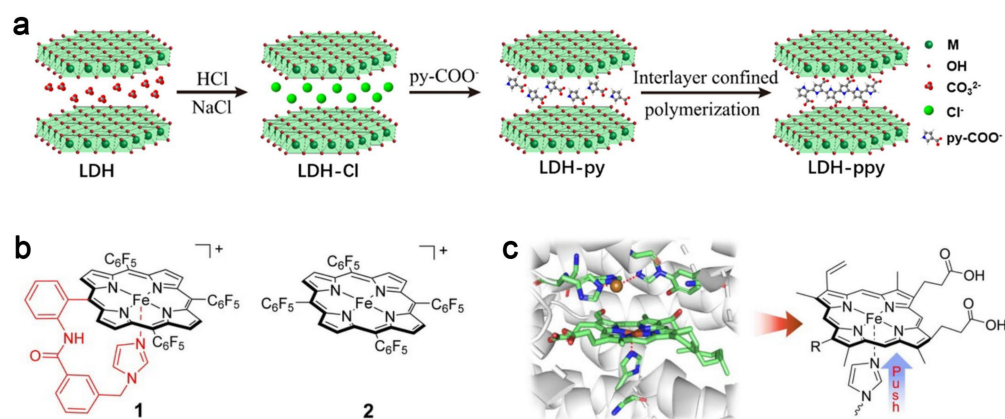


Figure 8. (a) Synthesis processes including anion exchange and interlayer confined polymerization for the preparation of LDH-ppy by Ju et al. [98]. Copyright © 2021, American Chemical Society. (b) Molecular structure of the two different Fe-porphyrins (1, 2) synthesized by Xie et al. [102]. (c) Diagram showing the electronic “push effect” of the trans axial histidine imidazole group in CcOs. Copyright © 2021, Wiley-VCH GmbH.

In addition to the oxidation states of transition metal ions, the spin states of the electrons in the orbitals also affect the electronic structure and, hence, influence the electrocatalytic activity of catalysts with transition metal ions as the active centers [119]. In 2022, Liang et al. [120] investigated the role of thiadiazole-[7] helicene, which is a chiral molecule, on modulating the catalytic performance of NiO_x/Au or NiFeO_x/Au by depositing monolayer NiO_x and NiFeO_x islands on the Au film. The chiral molecule was loaded on the surface of Au film just underlying the NiO_x or NiFeO_x catalyst layer. By evaluating the OER performance of the hybrids with and without the chiral molecule, the authors revealed that the positive effects of the chiral thiadiazole-[7] helicene on catalytic properties was not arising from the thiadiazole groups that directly affected the metal sites, but it was the existence of the chiral molecule itself that impacted the spin polarization of the electrons. The relationship between the spin of electrons and catalytic performance was also studied by using two different Fe-porphyrins [102]. As illustrated in Figure 8b, the difference between the delicately designed two Fe-porphyrins was that the one had an additional imidazole group (red molecule in Figure 8b) coordination, leading to a similar coordination structure of Fe ions to that in cytochrome *c* oxidases (CcOs), in which the electron density on Fe is increased through a so-called “push effect” (Figure 8c). According to the electron paramagnetic resonance (EPR) spectra, the electrons of Fe in Fe-porphyrin with an imidazole group, existed in both the high-spin and low-spin states, while only the high-spin state was observed in Fe-porphyrin without the imidazole group. And a dynamic equilibrium of Fe species between 6-coordinated high-spin and 5-coordinated low-spin states was proposed to accelerate the OER kinetics. These results give another way to tune the electronic structure of transition metal ions and then make the elemental component modulation of catalyst materials to go beyond the volcano limits.

4. Summary and Perspectives

OIHs are new kinds of emerging functional materials that have abundant nanoscale interfaces and redox properties, making them promising in electrocatalysis. This review has summarized the advances in fabrication, modification and application of typical OIHs including MOFs and their derivatives, COF-based hybrids, and other rationally designed OIHs. The well-designed organic molecules could be evenly dispersed and interact with transition metal centers in the inorganic counterpart, greatly influencing the coordination environments of active sites and leading to advanced catalytic performance towards water oxidation. Though many achievements have been realized, the research of OIHs for water

oxidation is still at its early stage and the challenges as well as the future research directions to address and deal with these limitations are listed below.

- (1) Rational design and fabrication of OIHs. The chemical compositions including both organic molecules and transition metal-based inorganic compounds in the reported OIHs are limited, while they are critical to determine the OER activity of the hybrids. Consequently, developing a universal and controllable method to fabricate the targeted OIH hybrids with high quality and in large scale is required in further studies. What's more, efforts should be made to expand the chemical composition of OIHs, enabling the synthesis of a wider range of organic molecules and transition metal-based inorganic compounds. This will facilitate the creation of highly tailored and functional materials.
- (2) Developing OIHs for efficient OER in low-pH conditions. In most OIHs, the active metal sites are immobilized through relatively weak chemical bonds, leading to their vulnerability in excessive acidic conditions. This is the reason why the majority of currently available OIHs function effectively only in alkaline environments. However, in terms of cost and safety, expanding the application of OIHs as OER catalysts that work well in acidic or neutral mediums is important [121]. To this end, the structure–performance relationship and reaction mechanism of OIHs towards OER should be identified to expand the application environments. The structure of the active center should be carefully determined, and the in situ techniques should be coupled with computational modelling to obtain the dynamic structural evolution of active centers in acidic or neutral electrolytes. This knowledge will guide the design of novel acidic-resistant OIHs with enhanced performance.
- (3) Understanding the low stability of OIHs. Although thousands of OIHs have been reported as OER electrocatalysts, most of them suffer from poor stability, especially under harsh reaction conditions. However, little in-depth research has been conducted on revealing the underlying reasons, leaving significant room for further interpretation. Several factors are suggested to be considered in future studies: (a) The effect of strong alkaline solutions. This consideration is important as the harsh environment may contribute to the collapse of the crystal structure and the coordination bonds in OIHs. (b) The potential applied during the OER process. The high positive potential to meet the high current density requirement would lead to the oxidation of organic components in OIHs that should be carefully determined. Note that measuring the Faradaic efficiency of O_2 is a helpful method to identify the accurate current density from water oxidation and provides some hints to the stability of organic components in OIHs, which should be highlighted when comparing the catalytic performance of OIHs in future investigations.

Author Contributions: Conceptualization, Z.T. and X.L.; investigation, X.L.; writing, Z.T.; review and editing, Z.T., L.Z., T.W., Y.Z., B.Z., Y.D. and X.L. All authors have read and agreed to the published version of the manuscript.

Funding: The authors appreciate the financial support from Shanghai Jiao Tong University (WH220828001 and ZXDF280001).

Data Availability Statement: No new data were created.

Conflicts of Interest: The authors declare no conflict of interest.

Abbreviations

AEM	adsorbates evolution mechanism
AFM	atomic force microscopy
BDC	benzenedicarboxylic acid
BPTC	biphenyl-3,4',5-tricarboxylic acid
BTC	benzenedicarboxylic acid
CC	carbon cloth
CNT	carbon nanotubes
COF	covalent organic frameworks
CV	cyclic voltametric
C _{dl}	electrochemical double-layer capacitance
EPR	electron paramagnetic resonance
EQCM-D	electrochemical quartz crystal microbalance with dissipation
EXAFS	extended X-ray absorption fine structure
FE	Faradaic efficiency
GC	glass carbon
GO	graphene oxide
HER	hydrogen evolution reaction
HRTEM	high-resolution transmission electron microscopy
LOM	lattice-oxygen participated mechanism
MOF	metal organic frameworks
MPN	metal-polyphenolic network
NB	nanoboxes
NF	nickel foam
NFF	nickel iron foam
OER	oxygen evolution reaction
OIH	organic-inorganic hybrid materials
RHE	reversible hydrogen electrode
SECM	scanning electrochemical microscopy
SEM	scanning electron microscopy
SSS	stainless steel strip
TA	tannic acid
TM	transition metals
XAS	synchrotron X-ray absorption spectroscopy
ZIF	zeolitic imidazolate frameworks
η	overpotential
b	Tafel slope

References

1. Ma, J.; Wang, J.; Li, J.; Tian, Y.; Zhang, T. A Green Synthesis Strategy for Cobalt Phosphide Deposited on N, P Co-Doped Graphene for Efficient Hydrogen Evolution. *Materials* **2023**, *16*, 6119. [[CrossRef](#)] [[PubMed](#)]
2. Ifkovits, Z.P.; Evans, J.M.; Meier, M.C.; Papadantonakis, K.M.; Lewis, N.S. Decoupled electrochemical water-splitting systems: A review and perspective. *Energy Environ. Sci.* **2021**, *14*, 4740–4759. [[CrossRef](#)]
3. Pleshivtseva, Y.; Derevyanov, M.; Pimenov, A.; Rapoport, A. Comparative analysis of global trends in low carbon hydrogen production towards the decarbonization pathway. *Int. J. Hydrogen Energy* **2023**, *48*, 32191–32240. [[CrossRef](#)]
4. Yu, W.; Liu, H.; Zhao, Y.; Fu, Y.; Xiao, W.; Dong, B.; Wu, Z.; Chai, Y.; Wang, L. Amorphous NiO_n coupled with trace PtO_x toward superior electrocatalytic overall water splitting in alkaline seawater media. *Nano Res.* **2023**, *16*, 6517–6530. [[CrossRef](#)]
5. Tan, Z.; Zhang, L.; Wu, T.; Zhou, B.; Long, X. Composition Tuned Electron Rearrangement of Transition-Metal-Based Compounds Promotes Hydrogen Generation. *J. Phys. Chem. C* **2023**, *127*, 15747–15756. [[CrossRef](#)]
6. Song, F.; Bai, L.; Moysiadou, A.; Lee, S.; Hu, C.; Liardet, L.; Hu, X. Transition Metal Oxides as Electrocatalysts for the Oxygen Evolution Reaction in Alkaline Solutions: An Application-Inspired Renaissance. *J. Am. Chem. Soc.* **2018**, *140*, 7748–7759. [[CrossRef](#)]
7. Yan, Z.; Liu, H.; Hao, Z.; Yu, M.; Chen, X.; Chen, J. Electrodeposition of (hydro)oxides for an oxygen evolution electrode. *Chem. Sci.* **2020**, *11*, 10614–10625. [[CrossRef](#)]
8. Long, X.; Ma, Z.; Yu, H.; Gao, X.; Pan, X.; Chen, X.; Yang, S.; Yi, Z. Porous FeNi oxide nanosheets as advanced electrochemical catalysts for sustained water oxidation. *J. Mater. Chem. A* **2016**, *4*, 14939–14943. [[CrossRef](#)]

9. Long, X.; Lin, H.; Zhou, D.; An, Y.; Yang, S. Enhancing full water-splitting performance of transition metal bifunctional electrocatalysts in alkaline solutions by tailoring CeO₂-transition metal oxides-Ni nanointerfaces. *ACS Energy Lett.* **2018**, *3*, 290–296. [[CrossRef](#)]
10. Alobaid, A.; Wang, C.; Adomaitis, R.A. Mechanism and Kinetics of HER and OER on NiFe LDH Films in an Alkaline Electrolyte. *J. Electrochem. Soc.* **2018**, *165*, J3395. [[CrossRef](#)]
11. Zhou, D.; Li, P.; Lin, X.; McKinley, A.; Kuang, Y.; Liu, W.; Lin, W.F.; Sun, X.; Duan, X. Layered double hydroxide-based electrocatalysts for the oxygen evolution reaction: Identification and tailoring of active sites, and superaerophobic nanoarray electrode assembly. *Chem. Soc. Rev.* **2021**, *50*, 8790–8817. [[CrossRef](#)] [[PubMed](#)]
12. Ju, M.; Chen, Z.; Zhu, H.; Cai, R.; Lin, Z.; Chen, Y.; Wang, Y.; Gao, J.; Long, X.; Yang, S. Fe (III) Docking-Activated Sites in Layered Birnessite for Efficient Water Oxidation. *J. Am. Chem. Soc.* **2023**, *145*, 11215–11226. [[CrossRef](#)] [[PubMed](#)]
13. Hameed, A.; Batool, M.; Liu, Z.; Nadeem, M.A.; Jin, R. Layered Double Hydroxide-Derived Nanomaterials for Efficient Electrocatalytic Water Splitting: Recent Progress and Future Perspective. *ACS Energy Lett.* **2022**, *7*, 3311–3328. [[CrossRef](#)]
14. Zhao, Y.; Wen, Q.; Huang, D.; Jiao, C.; Liu, Y.; Liu, Y.; Fang, J.; Sun, M.; Yu, L. Operando Reconstruction toward Dual-Cation-Defects Co-Containing NiFe Oxyhydroxide for Ultralow Energy Consumption Industrial Water Splitting Electrolyzer. *Adv. Energy Mater.* **2023**, *13*, 2203595. [[CrossRef](#)]
15. Zhang, B.; Wang, L.; Cao, Z.; Kozlov, S.M.; García de Arquer, F.P.; Dinh, C.T.; Li, J.; Wang, Z.; Zheng, X.; Zhang, L.; et al. High-valence metals improve oxygen evolution reaction performance by modulating 3d metal oxidation cycle energetics. *Nat. Catal.* **2020**, *3*, 985–992. [[CrossRef](#)]
16. Zhang, H.; Maijenburg, A.W.; Li, X.; Schweizer, S.L.; Wehrspohn, R.B. Bifunctional Heterostructured Transition Metal Phosphides for Efficient Electrochemical Water Splitting. *Adv. Funct. Mater.* **2020**, *30*, 2003261. [[CrossRef](#)]
17. Zhao, H.; Yuan, Z.-Y. Transition metal-phosphorus-based materials for electrocatalytic energy conversion reactions. *Catal. Sci. Technol.* **2017**, *7*, 330–347. [[CrossRef](#)]
18. Su, J.; Zhou, J.; Wang, L.; Liu, C.; Chen, Y. Synthesis and application of transition metal phosphides as electrocatalyst for water splitting. *Sci. Bull.* **2017**, *62*, 633–644. [[CrossRef](#)]
19. Cai, R.; Ju, M.; Chen, J.; Ren, J.; Yu, J.; Long, X.; Yang, S. Recent advances in surface/interface engineering of noble-metal free catalysts for energy conversion reactions. *Mater. Chem. Front.* **2021**, *5*, 3576–3592. [[CrossRef](#)]
20. Long, X.; Qiu, W.; Wang, Z.; Wang, Y.; Yang, S. Recent advances in transition metal-based catalysts with heterointerfaces for energy conversion and storage. *Mater. Today Chem.* **2019**, *11*, 16–28. [[CrossRef](#)]
21. Alemán, J.V.; Chadwick, A.V.; He, J.; Hess, M.; Horie, K.; Jones, R.G.; Kratochvíl, P.; Meisel, I.; Mita, I.; Moad, G.; et al. Definitions of terms relating to the structure and processing of sols, gels, networks, and inorganic-organic hybrid materials (IUPAC Recommendations 2007). *Pure Appl. Chem.* **2007**, *79*, 1801–1829. [[CrossRef](#)]
22. Li, W.; Zhang, S.; Zheng, W.; Ma, J.; Li, L.; Zheng, Y.; Sun, D.; Wen, Z.; Liu, Z.; Wang, Y.; et al. Self-Polarized Organic-Inorganic Hybrid Ferroelectric Cathode Coatings Assisted High Performance All-Solid-State Lithium Battery. *Adv. Funct. Mater.* **2023**, *33*, 2300791. [[CrossRef](#)]
23. Ma, X.; Cao, X.; Yao, M.; Shan, L.; Shi, X.; Fang, G.; Pan, A.; Lu, B.; Zhou, J.; Liang, S. Organic-Inorganic Hybrid Cathode with Dual Energy-Storage Mechanism for Ultrahigh-Rate and Ultralong-Life Aqueous Zinc-Ion Batteries. *Adv. Mater.* **2022**, *34*, 2105452. [[CrossRef](#)] [[PubMed](#)]
24. Pettinari, C.; Tombesi, A. MOFs for Electrochemical Energy Conversion and Storage. *Inorganics* **2023**, *11*, 65. [[CrossRef](#)]
25. Ren, Z.; Yang, J.; Qi, D.; Sonar, P.; Liu, L.; Lou, Z.; Shen, G.; Wei, Z. Flexible Sensors Based on Organic-Inorganic Hybrid Materials. *Adv. Mater. Technol.* **2021**, *6*, 2000889. [[CrossRef](#)]
26. Li, D.; Jia, Z.; Tang, Y.; Song, C.; Liang, K.; Ren, H.; Li, F.; Chen, Y.; Wang, Y.; Lu, X.; et al. Inorganic-Organic Hybrid Phototransistor Array with Enhanced Photogating Effect for Dynamic Near-Infrared Light Sensing and Image Preprocessing. *Nano Lett.* **2022**, *22*, 5434–5442. [[CrossRef](#)]
27. Kladsomboon, S.; Thippakorn, C.; Seesaard, T. Development of Organic-Inorganic Hybrid Optical Gas Sensors for the Non-Invasive Monitoring of Pathogenic Bacteria. *Sensors* **2018**, *18*, 3189. [[CrossRef](#)]
28. Goodman, E.D.; Zhou, C.; Cargnello, M. Design of Organic/Inorganic Hybrid Catalysts for Energy and Environmental Applications. *ACS Cent. Sci.* **2020**, *6*, 1916–1937. [[CrossRef](#)]
29. Zhang, H.; Chen, L.; Li, Y.; Hu, Y.; Li, H.; Xu, C.C.; Yang, S. Functionalized organic-inorganic hybrid porous coordination polymer-based catalysts for biodiesel production via trans/esterification. *Green Chem.* **2022**, *24*, 7763–7786. [[CrossRef](#)]
30. Erigoni, A.; Diaz, U. Porous Silica-Based Organic-Inorganic Hybrid Catalysts: A Review. *Catalysts* **2021**, *11*, 79. [[CrossRef](#)]
31. Lei, Z.; Cai, W.; Rao, Y.; Wang, K.; Jiang, Y.; Liu, Y.; Jin, X.; Li, J.; Lv, Z.; Jiao, S.; et al. Coordination modulation of iridium single-atom catalyst maximizing water oxidation activity. *Nat. Commun.* **2022**, *13*, 24. [[CrossRef](#)] [[PubMed](#)]
32. Li, L.; Wang, P.; Shao, Q.; Huang, X. Metallic nanostructures with low dimensionality for electrochemical water splitting. *Chem. Soc. Rev.* **2020**, *49*, 3072–3106. [[CrossRef](#)] [[PubMed](#)]
33. Rossmeisl, J.; Logadottir, A.; Nørskov, J.K. Electrolysis of water on (oxidized) metal surfaces. *Chem. Phys.* **2005**, *319*, 178–184. [[CrossRef](#)]
34. Gomez, R.; Fernandez-Vega, A.; Feliu, J.M.; Aldaz, A. Hydrogen evolution on platinum single crystal surfaces: Effects of irreversibly adsorbed bismuth and antimony on hydrogen adsorption and evolution on platinum (100). *J. Phys. Chem.* **1993**, *97*, 4769–4776. [[CrossRef](#)]

35. Grimaud, A.; Diaz-Morales, O.; Han, B.; Hong, W.T.; Lee, Y.-L.; Giordano, L.; Stoerzinger, K.A.; Koper, M.T.M.; Shao-Horn, Y. Activating lattice oxygen redox reactions in metal oxides to catalyse oxygen evolution. *Nat. Chem.* **2017**, *9*, 457–465. [[CrossRef](#)]
36. Reier, T.; Nong, H.N.; Teschner, D.; Schlögl, R.; Strasser, P. Electrocatalytic Oxygen Evolution Reaction in Acidic Environments—Reaction Mechanisms and Catalysts. *Adv. Energy Mater.* **2017**, *7*, 1601275. [[CrossRef](#)]
37. Zhang, N.; Chai, Y. Lattice oxygen redox chemistry in solid-state electrocatalysts for water oxidation. *Energy Environ. Sci.* **2021**, *14*, 4647–4671. [[CrossRef](#)]
38. Nørskov, J.K.; Rossmeisl, J.; Logadottir, A.; Lindqvist, L.; Kitchin, J.R.; Bligaard, T.; Jónsson, H. Origin of the Overpotential for Oxygen Reduction at a Fuel-Cell Cathode. *J. Phys. Chem. B* **2004**, *108*, 17886–17892. [[CrossRef](#)]
39. Abild-Pedersen, F.; Greeley, J.; Studt, F.; Rossmeisl, J.; Munter, T.R.; Moses, P.G.; Skúlason, E.; Bligaard, T.; Nørskov, J.K. Scaling Properties of Adsorption Energies for Hydrogen-Containing Molecules on Transition-Metal Surfaces. *Phys. Rev. Lett.* **2007**, *99*, 016105. [[CrossRef](#)]
40. Greeley, J. Theoretical Heterogeneous Catalysis: Scaling Relationships and Computational Catalyst Design. *Annu. Rev. Chem. Biomol. Eng.* **2016**, *7*, 605–635. [[CrossRef](#)]
41. Seh, Z.W.; Kibsgaard, J.; Dickens, C.F.; Chorkendorff, I.; Nørskov, J.K.; Jaramillo, T.F. Combining theory and experiment in electrocatalysis: Insights into materials design. *Science* **2017**, *355*, eaad4998. [[CrossRef](#)]
42. Calle-Vallejo, F.; Loffreda, D.; Koper, M.T.M.; Sautet, P. Introducing structural sensitivity into adsorption–energy scaling relations by means of coordination numbers. *Nat. Chem.* **2015**, *7*, 403–410. [[CrossRef](#)]
43. Zhang, Y.; Li, Z.; Zhang, K.; Wu, Z.; Gao, F.; Du, Y. Heterogeneous interface engineering for boosting electron transfer induced by MOF-derived Yolk-shell trimetallic phosphide nanospindles for robust water oxidation electrocatalysis. *Appl. Surf. Sci.* **2022**, *590*, 153102. [[CrossRef](#)]
44. Liu, X.; You, B.; Yu, X.-Y.; Chipman, J.; Sun, Y. Electrochemical oxidation to construct a nickel sulfide/oxide heterostructure with improvement of capacitance. *J. Mater. Chem. A* **2016**, *4*, 11611–11615. [[CrossRef](#)]
45. Wohlfahrt-Mehrens, M.; Heitbaum, J. Oxygen evolution on Ru and RuO₂ electrodes studied using isotope labelling and on-line mass spectrometry. *J. Electroanal. Chem. Interfacial Electrochem.* **1987**, *237*, 251–260. [[CrossRef](#)]
46. Tyburski, R.; Liu, T.; Glover, S.D.; Hammarström, L. Proton-Coupled Electron Transfer Guidelines, Fair and Square. *J. Am. Chem. Soc.* **2021**, *143*, 560–576. [[CrossRef](#)]
47. Chen, F.-Y.; Wu, Z.-Y.; Adler, Z.; Wang, H. Stability challenges of electrocatalytic oxygen evolution reaction: From mechanistic understanding to reactor design. *Joule* **2021**, *5*, 1704–1731. [[CrossRef](#)]
48. Anantharaj, S.; Sugime, H.; Noda, S. Why shouldn't double-layer capacitance (C_{dl}) be always trusted to justify Faradaic electrocatalytic activity differences? *J. Electroanal. Chem.* **2021**, *903*, 115842. [[CrossRef](#)]
49. Shin, S.-J.; Kim, D.H.; Bae, G.; Ringe, S.; Choi, H.; Lim, H.-K.; Choi, C.H.; Kim, H. On the importance of the electric double layer structure in aqueous electrocatalysis. *Nat. Commun.* **2022**, *13*, 174. [[CrossRef](#)]
50. Wang, M.; Zhang, L.; He, Y.; Zhu, H. Recent advances in transition-metal-sulfide-based bifunctional electrocatalysts for overall water splitting. *J. Mater. Chem. A* **2021**, *9*, 5320–5363. [[CrossRef](#)]
51. Zhou, H.; Li, Z.; Xu, S.-M.; Lu, L.; Xu, M.; Ji, K.; Ge, R.; Yan, Y.; Ma, L.; Kong, X.; et al. Selectively Upgrading Lignin Derivatives to Carboxylates through Electrochemical Oxidative C(OH)–C Bond Cleavage by a Mn-Doped Cobalt Oxyhydroxide Catalyst. *Angew. Chem. Int. Ed.* **2021**, *60*, 8976–8982. [[CrossRef](#)]
52. Kempler, P.A.; Nielander, A.C. Reliable reporting of Faradaic efficiencies for electrocatalysis research. *Nat. Commun.* **2023**, *14*, 1158. [[CrossRef](#)]
53. Yaghi, O.M.; Li, G.; Li, H. Selective binding and removal of guests in a microporous metal-organic framework. *Nature* **1995**, *378*, 703–706. [[CrossRef](#)]
54. Eddaoudi, M.; Kim, J.; Rosi, N.; Vodak, D.; Wachter, J.; O'Keeffe, M.; Yaghi, O.M. Systematic Design of Pore Size and Functionality in Isoreticular MOFs and Their Application in Methane Storage. *Science* **2002**, *295*, 469–472. [[CrossRef](#)]
55. Park, K.S.; Ni, Z.; Côté, A.P.; Choi, J.Y.; Huang, R.; Uribe-Romo, F.J.; Chae, H.K.; O'Keeffe, M.; Yaghi, O.M. Exceptional chemical and thermal stability of zeolitic imidazolate frameworks. *Proc. Natl. Acad. Sci. USA* **2006**, *103*, 10186–10191. [[CrossRef](#)]
56. Férey, G.; Mellot-Draznieks, C.; Serre, C.; Millange, F.; Dutour, J.; Surblé, S.; Margiolaki, I. A Chromium Terephthalate-Based Solid with Unusually Large Pore Volumes and Surface Area. *Science* **2005**, *309*, 2040–2042. [[CrossRef](#)]
57. Qiu, S.; Xue, M.; Zhu, G. Metal-organic framework membranes: From synthesis to separation application. *Chem. Soc. Rev.* **2014**, *43*, 6116–6140. [[CrossRef](#)]
58. Fan, W.; Zhang, X.; Kang, Z.; Liu, X.; Sun, D. Isoreticular chemistry within metal-organic frameworks for gas storage and separation. *Coord. Chem. Rev.* **2021**, *443*, 213968. [[CrossRef](#)]
59. Jia, T.; Gu, Y.; Li, F. Progress and potential of metal-organic frameworks (MOFs) for gas storage and separation: A review. *J. Environ. Chem. Eng.* **2022**, *10*, 108300. [[CrossRef](#)]
60. Denny, M.S., Jr.; Moreton, J.C.; Benz, L.; Cohen, S.M. Metal-organic frameworks for membrane-based separations. *Nat. Rev. Mater.* **2016**, *1*, 16078. [[CrossRef](#)]
61. Uddin, M.J.; Ampia, R.E.; Lee, W. Adsorptive removal of dyes from wastewater using a metal-organic framework: A review. *Chemosphere* **2021**, *284*, 131314. [[CrossRef](#)]
62. Sanati, S.; Morsali, A.; Garcia, H. First-row transition metal-based materials derived from bimetallic metal-organic frameworks as highly efficient electrocatalysts for electrochemical water splitting. *Energy Environ. Sci.* **2022**, *15*, 3119–3151. [[CrossRef](#)]

63. Carson, F.; Agrawal, S.; Gustafsson, M.; Bartoszewicz, A.; Moraga, F.; Zou, X.; Martin-Matute, B. Ruthenium Complexation in an Aluminium Metal-Organic Framework and Its Application in Alcohol Oxidation Catalysis. *Chem.-A Eur. J.* **2012**, *18*, 15337–15344. [[CrossRef](#)]
64. Khan, I.S.; Garzon-Tovar, L.; Mateo, D.; Gascon, J. Metal-Organic-Frameworks and Their Derived Materials in Photo-Thermal Catalysis. *Eur. J. Inorg. Chem.* **2022**, *2022*, e202200316. [[CrossRef](#)]
65. Xuan, X.; Chen, S.; Zhao, S.; Yoon, J.Y.; Boczkaj, G.; Sun, X. Carbon Nanomaterials From Metal-Organic Frameworks: A New Material Horizon for CO₂ Reduction. *Front. Chem.* **2020**, *8*, 573797. [[CrossRef](#)]
66. Han, A.; Wang, B.; Kumar, A.; Qin, Y.; Jin, J.; Wang, X.; Yang, C.; Dong, B.; Jia, Y.; Liu, J.; et al. Recent Advances for MOF-Derived Carbon-Supported Single-Atom Catalysts. *Small Methods* **2019**, *3*, 1800471. [[CrossRef](#)]
67. He, S.; Wu, L.; Li, X.; Sun, H.; Xiong, T.; Liu, J.; Huang, C.; Xu, H.; Sun, H.; Chen, W.; et al. Metal-organic frameworks for advanced drug delivery. *Acta Pharm. Sin. B* **2021**, *11*, 2362–2395. [[CrossRef](#)]
68. Peng, Y.; Sanati, S.; Morsali, A.; Garcia, H. Metal-Organic Frameworks as Electrocatalysts. *Angew. Chem. Int. Ed. Engl.* **2023**, *62*, e202214707. [[CrossRef](#)]
69. Zhao, S.; Wang, Y.; Dong, J.; He, C.-T.; Yin, H.; An, P.; Zhao, K.; Zhang, X.; Gao, C.; Zhang, L.; et al. Ultrathin metal-organic framework nanosheets for electrocatalytic oxygen evolution. *Nat. Energy* **2016**, *1*, 16184. [[CrossRef](#)]
70. Ge, K.; Sun, S.; Zhao, Y.; Yang, K.; Wang, S.; Zhang, Z.; Cao, J.; Yang, Y.; Zhang, Y.; Pan, M.; et al. Facile Synthesis of Two-Dimensional Iron/Cobalt Metal-Organic Framework for Efficient Oxygen Evolution Electrocatalysis. *Angew. Chem. Int. Ed.* **2021**, *60*, 12097–12102. [[CrossRef](#)]
71. Cao, C.; Ma, D.D.; Xu, Q.; Wu, X.T.; Zhu, Q.L. Semisacrificial Template Growth of Self-Supporting MOF Nanocomposite Electrode for Efficient Electrocatalytic Water Oxidation. *Adv. Funct. Mater.* **2018**, *29*, 1807418. [[CrossRef](#)]
72. Li, W.; Fang, W.; Wu, C.; Dinh, K.N.; Ren, H.; Zhao, L.; Liu, C.; Yan, Q. Bimetal-MOF nanosheets as efficient bifunctional electrocatalysts for oxygen evolution and nitrogen reduction reaction. *J. Mater. Chem. A* **2020**, *8*, 3658–3666. [[CrossRef](#)]
73. Wang, C.-P.; Feng, Y.; Sun, H.; Wang, Y.; Yin, J.; Yao, Z.; Bu, X.-H.; Zhu, J. Self-Optimized Metal-Organic Framework Electrocatalysts with Structural Stability and High Current Tolerance for Water Oxidation. *ACS Catal.* **2021**, *11*, 7132–7143. [[CrossRef](#)]
74. Zhao, S.; Tan, C.; He, C.-T.; An, P.; Xie, F.; Jiang, S.; Zhu, Y.; Wu, K.-H.; Zhang, B.; Li, H.; et al. Structural transformation of highly active metal-organic framework electrocatalysts during the oxygen evolution reaction. *Nat. Energy* **2020**, *5*, 881–890. [[CrossRef](#)]
75. Wang, X.-L.; Dong, L.-Z.; Qiao, M.; Tang, Y.-J.; Liu, J.; Li, Y.; Li, S.-L.; Su, J.-X.; Lan, Y.-Q. Exploring the Performance Improvement of the Oxygen Evolution Reaction in a Stable Bimetal-Organic Framework System. *Angew. Chem. Int. Ed.* **2018**, *57*, 9660–9664. [[CrossRef](#)]
76. Zhou, W.; Huang, D.-D.; Wu, Y.-P.; Zhao, J.; Wu, T.; Zhang, J.; Li, D.-S.; Sun, C.; Feng, P.; Bu, X. Stable Hierarchical Bimetal-Organic Nanostructures as High-Performance Electrocatalysts for the Oxygen Evolution Reaction. *Angew. Chem. Int. Ed.* **2019**, *58*, 4227–4231. [[CrossRef](#)]
77. Yan, L.; Xu, Y.; Chen, P.; Zhang, S.; Jiang, H.; Yang, L.; Wang, Y.; Zhang, L.; Shen, J.; Zhao, X.; et al. A Freestanding 3D Heterostructure Film Stitched by MOF-Derived Carbon Nanotube Microsphere Superstructure and Reduced Graphene Oxide Sheets: A Superior Multifunctional Electrode for Overall Water Splitting and Zn-Air Batteries. *Adv. Mater.* **2020**, *32*, e2003313. [[CrossRef](#)]
78. Jia, X.; Wu, J.; Lu, K.; Li, Y.; Qiao, X.; Kaelin, J.; Lu, S.; Cheng, Y.; Wu, X.; Qin, W. Organic-inorganic hybrids of Fe-Co polyphenolic network wrapped Fe₃O₄ nanocatalysts for significantly enhanced oxygen evolution. *J. Mater. Chem. A* **2019**, *7*, 14302–14308. [[CrossRef](#)]
79. Huang, Y.; Zhang, S.L.; Lu, X.F.; Wu, Z.-P.; Luan, D.; Lou, X.W. Trimetallic Spinel NiCo_{2-x}Fe_xO₄ Nanoboxes for Highly Efficient Electrocatalytic Oxygen Evolution. *Angew. Chem. Int. Ed.* **2021**, *60*, 11841–11846. [[CrossRef](#)]
80. Mesbah, A.; Rabu, P.; Sibille, R.; Lebègue, S.; Mazet, T.; Malaman, B.; François, M. From Hydrated Ni₃(OH)₂(C₈H₄O₄)₂(H₂O)₄ to Anhydrous Ni₂(OH)₂(C₈H₄O₄): Impact of Structural Transformations on Magnetic Properties. *Inorg. Chem.* **2014**, *53*, 872–881. [[CrossRef](#)]
81. Carton, A.; Mesbah, A.; Mazet, T.; Porcher, F.; François, M. Ab initio crystal structure of nickel(II) hydroxy-terephthalate by synchrotron powder diffraction and magnetic study. *Solid State Sci.* **2007**, *9*, 465–471. [[CrossRef](#)]
82. Jin, S. How to Effectively Utilize MOFs for Electrocatalysis. *ACS Energy Lett.* **2019**, *4*, 1443–1445. [[CrossRef](#)]
83. Li, H.; Eddaoudi, M.; O’Keeffe, M.; Yaghi, O.M. Design and synthesis of an exceptionally stable and highly porous metal-organic framework. *Nature* **1999**, *402*, 276–279. [[CrossRef](#)]
84. Côté, A.P.; Benin, A.I.; Ockwig, N.W.; O’Keeffe, M.; Matzger, A.J.; Yaghi, O.M. Porous, Crystalline, Covalent Organic Frameworks. *Science* **2005**, *310*, 1166–1170. [[CrossRef](#)]
85. Chakraborty, D.; Mullangi, D.; Chandran, C.; Vaidhyanathan, R. Nanopores of a Covalent Organic Framework: A Customizable Vessel for Organocatalysis. *ACS Omega* **2022**, *7*, 15275–15295. [[CrossRef](#)]
86. Ding, S.-Y.; Gao, J.; Wang, Q.; Zhang, Y.; Song, W.-G.; Su, C.-Y.; Wang, W. Construction of Covalent Organic Framework for Catalysis: Pd/COF-LZU1 in Suzuki-Miyaura Coupling Reaction. *J. Am. Chem. Soc.* **2011**, *133*, 19816–19822. [[CrossRef](#)]
87. Mullangi, D.; Dhavale, V.; Shalini, S.; Nandi, S.; Collins, S.; Woo, T.; Kurungot, S.; Vaidhyanathan, R. Low-Overpotential Electrocatalytic Water Splitting with Noble-Metal-Free Nanoparticles Supported in a sp³ N-Rich Flexible COF. *Adv. Energy Mater.* **2016**, *6*, 1600110. [[CrossRef](#)]

88. Nandi, S.; Singh, S.K.; Mullangi, D.; Illathvalappil, R.; George, L.; Vinod, C.P.; Kurungot, S.; Vaidhyanathan, R. Low Band Gap Benzimidazole COF Supported Ni₃N as Highly Active OER Catalyst. *Adv. Energy Mater.* **2016**, *6*, 1601189. [[CrossRef](#)]
89. Lyu, H.; Diercks, C.S.; Zhu, C.; Yaghi, O.M. Porous Crystalline Olefin-Linked Covalent Organic Frameworks. *J. Am. Chem. Soc.* **2019**, *141*, 6848–6852. [[CrossRef](#)]
90. Zhang, N.; Yang, Z.; Liu, W.; Zhang, F.; Yan, H. Novel Bifunctional Nitrogen Doped MoS₂/COF-C₄N Vertical Heterostructures for Electrocatalytic HER and OER. *Catalysts* **2023**, *13*, 90. [[CrossRef](#)]
91. Zhang, R.; Liu, W.; Zhang, F.-M.; Yang, Z.-D.; Zhang, G.; Zeng, X.C. COF-C₄N Nanosheets with uniformly anchored single metal sites for electrocatalytic OER: From theoretical screening to target synthesis. *Appl. Catal. B Environ.* **2023**, *325*, 122366. [[CrossRef](#)]
92. Gao, Z.; Yu, Z.; Huang, Y.; He, X.; Su, X.; Xiao, L.; Yu, Y.; Huang, X.; Luo, F. Flexible and robust bimetallic covalent organic frameworks for the reversible switching of electrocatalytic oxygen evolution activity. *J. Mater. Chem. A* **2020**, *8*, 5907–5912. [[CrossRef](#)]
93. Feng, X.; Gao, Z.; Xiao, L.; Lai, Z.; Luo, F. A Ni/Fe complex incorporated into a covalent organic framework as a single-site heterogeneous catalyst for efficient oxygen evolution reaction. *Inorg. Chem. Front.* **2020**, *7*, 3925–3931. [[CrossRef](#)]
94. Zong, H.; Liu, W.; Li, M.; Gong, S.; Yu, K.; Zhu, Z. Oxygen-Terminated Nb₂CO₂ MXene with Interfacial Self-Assembled COF as a Bifunctional Catalyst for Durable Zinc-Air Batteries. *ACS Appl. Mater. Interfaces* **2022**, *14*, 10738–10746. [[CrossRef](#)]
95. Alsudairy, Z.; Brown, N.; Campbell, A.; Ambus, A.; Brown, B.; Smith-Petty, K.; Li, X. Covalent organic frameworks in heterogeneous catalysis: Recent advances and future perspective. *Mater. Chem. Front.* **2023**, *7*, 3298–3331. [[CrossRef](#)]
96. Peng, Y.; Hu, Z.; Gao, Y.; Yuan, D.; Kang, Z.; Qian, Y.; Yan, N.; Zhao, D. Synthesis of a Sulfonated Two-Dimensional Covalent Organic Framework as an Efficient Solid Acid Catalyst for Biobased Chemical Conversion. *ChemSusChem* **2015**, *8*, 3208–3212. [[CrossRef](#)]
97. Yang, C.; Yang, Z.-D.; Dong, H.; Sun, N.; Lu, Y.; Zhang, F.-M.; Zhang, G. Theory-Driven Design and Targeting Synthesis of a Highly-Conjugated Basal-Plane 2D Covalent Organic Framework for Metal-Free Electrocatalytic OER. *ACS Energy Lett.* **2019**, *4*, 2251–2258. [[CrossRef](#)]
98. Ju, M.; Cai, R.; Ren, J.; Chen, J.; Qi, L.; Long, X.; Yang, S. Conductive Polymer Intercalation Tunes Charge Transfer and Sorption-Desorption Properties of LDH Enabling Efficient Alkaline Water Oxidation. *ACS Appl. Mater. Interfaces* **2021**, *13*, 37063–37070. [[CrossRef](#)]
99. Aman, S.; Gouadria, S.; Manzoor, S.; Abdullah, M.; Khosa, R.Y.; Ashiq, M.N.; Ansari, M.Z.; Alfantazi, A. Facile synthesis of CuZrO₃@PPY nanohybrid balls embedded 3-dimensional network with synergistic effect for efficient oxygen evolution reaction. *Surf. Interfaces* **2023**, *36*, 102607. [[CrossRef](#)]
100. Lyu, S.; Guo, C.; Wang, J.; Li, Z.; Yang, B.; Lei, L.; Wang, L.; Xiao, J.; Zhang, T.; Hou, Y. Exceptional catalytic activity of oxygen evolution reaction via two-dimensional graphene multilayer confined metal-organic frameworks. *Nat. Commun.* **2022**, *13*, 6171. [[CrossRef](#)]
101. Li, H.; Li, X.; Lei, H.; Zhou, G.; Zhang, W.; Cao, R. Convenient Immobilization of Cobalt Corroles on Carbon Nanotubes through Covalent Bonds for Electrocatalytic Hydrogen and Oxygen Evolution Reactions. *ChemSusChem* **2019**, *12*, 801–806. [[CrossRef](#)] [[PubMed](#)]
102. Xie, L.; Zhang, X.-P.; Zhao, B.; Li, P.; Qi, J.; Guo, X.; Wang, B.; Lei, H.; Zhang, W.; Apfel, U.-P.; et al. Enzyme-Inspired Iron Porphyrins for Improved Electrocatalytic Oxygen Reduction and Evolution Reactions. *Angew. Chem.* **2021**, *133*, 7654–7659. [[CrossRef](#)]
103. Moulson, A.J. Transition Metal Oxides. In *Concise Encyclopedia of Advanced Ceramic Materials*; Brook, R.J., Ed.; Pergamon: Oxford, UK, 1991; pp. 497–499.
104. Walia, S.; Balendhran, S.; Nili, H.; Zhuyikov, S.; Rosengarten, G.; Wang, Q.H.; Bhaskaran, M.; Sriram, S.; Strano, M.S.; Kalantar-zadeh, K. Transition metal oxides—Thermoelectric properties. *Prog. Mater. Sci.* **2013**, *58*, 1443–1489. [[CrossRef](#)]
105. Lu, K.-Q.; Li, Y.-H.; Zhang, F.; Qi, M.-Y.; Chen, X.; Tang, Z.-R.; Yamada, Y.M.A.; Anpo, M.; Conte, M.; Xu, Y.-J. Rationally designed transition metal hydroxide nanosheet arrays on graphene for artificial CO₂ reduction. *Nat. Commun.* **2020**, *11*, 5181. [[CrossRef](#)] [[PubMed](#)]
106. Chen, H.; Zhang, P.; Xie, R.; Xiong, Y.; Jia, C.; Fu, Y.; Song, P.; Chen, L.; Zhang, Y.; Liao, T. High-Temperature Nitridation Induced Carbon Nanotubes@NiFe-Layered-Double-Hydroxide Nanosheets Taking as an Oxygen Evolution Reaction Electrocatalyst for CO₂ Electroreduction. *Adv. Mater. Interfaces* **2021**, *8*, 2101165. [[CrossRef](#)]
107. Duarte, M.F.P.; Rocha, I.M.; Figueiredo, J.L.; Freire, C.; Pereira, M.F.R. CoMn-LDH@carbon nanotube composites: Bifunctional electrocatalysts for oxygen reactions. *Catal. Today* **2018**, *301*, 17–24. [[CrossRef](#)]
108. Gong, M.; Li, Y.; Wang, H.; Liang, Y.; Wu, J.Z.; Zhou, J.; Wang, J.; Regier, T.; Wei, F.; Dai, H. An Advanced Ni-Fe Layered Double Hydroxide Electrocatalyst for Water Oxidation. *J. Am. Chem. Soc.* **2013**, *135*, 8452–8455. [[CrossRef](#)]
109. Long, X.; Li, J.; Xiao, S.; Yan, K.; Wang, Z.; Chen, H.; Yang, S. A Strongly Coupled Graphene and FeNi Double Hydroxide Hybrid as an Excellent Electrocatalyst for the Oxygen Evolution Reaction. *Angew. Chem.* **2014**, *126*, 7714–7718. [[CrossRef](#)]
110. Xu, X.; Chu, H.; Zhang, Z.; Dong, P.; Baines, R.; Ajayan, P.M.; Shen, J.; Ye, M. Integrated Energy Aerogel of N,S-rGO/WS₂/NiFe-LDH for Both Energy Conversion and Storage. *ACS Appl. Mater. Interfaces* **2017**, *9*, 32756–32766. [[CrossRef](#)]
111. Li, Y.; Wang, H.; Xie, L.; Liang, Y.; Hong, G.; Dai, H. MoS₂ Nanoparticles Grown on Graphene: An Advanced Catalyst for the Hydrogen Evolution Reaction. *J. Am. Chem. Soc.* **2011**, *133*, 7296–7299. [[CrossRef](#)]

112. Bai, X.; Cao, T.; Xia, T.; Wu, C.; Feng, M.; Li, X.; Mei, Z.; Gao, H.; Huo, D.; Ren, X.; et al. MoS₂/NiSe₂/rGO Multiple-Interfaced Sandwich-like Nanostructures as Efficient Electrocatalysts for Overall Water Splitting. *Nanomaterials* **2023**, *13*, 752. [[CrossRef](#)] [[PubMed](#)]
113. Lin, H.; Long, X.; An, Y.; Zhou, D.; Yang, S. Three-Dimensional Decoupling Co-Catalyst from a Photoabsorbing Semiconductor as a New Strategy To Boost Photoelectrochemical Water Splitting. *Nano Lett.* **2019**, *19*, 455–460. [[CrossRef](#)] [[PubMed](#)]
114. Li, W.; Wang, C.; Lu, X. Conducting polymers-derived fascinating electrocatalysts for advanced hydrogen and oxygen electrocatalysis. *Coord. Chem. Rev.* **2022**, *464*, 214555. [[CrossRef](#)]
115. Alsultan, M.; Ranjbar, A.; Swiegers, G.F.; Wallace, G.G.; Balakrishnan, S.; Huang, J. Application of Conducting Polymers in Solar Water-Splitting Catalysis. In *Industrial Applications for Intelligent Polymers and Coatings*; Hosseini, M., Makhlof, A.S.H., Eds.; Springer International Publishing: Cham, Switzerland, 2016; pp. 223–251.
116. Zhu, Y.; Liu, C.; Cui, S.; Lu, Z.; Ye, J.; Wen, Y.; Shi, W.; Huang, X.; Xue, L.; Bian, J.; et al. Multistep Dissolution of Lamellar Crystals Generates Superthin Amorphous Ni(OH)₂ Catalyst for UOR. *Adv. Mater.* **2023**, *35*, e2301549. [[CrossRef](#)]
117. Pang, A.L.; Arsad, A.; Ahmadipour, M. Synthesis and factor affecting on the conductivity of polypyrrole: A short review. *Polym. Adv. Technol.* **2021**, *32*, 1428–1454. [[CrossRef](#)]
118. Wolszczak, M.; Kroh, J.; Abdel-Hamid, M.M. Some aspects of the radiation processing of conducting polymers. *Radiat. Phys. Chem.* **1995**, *45*, 71–78. [[CrossRef](#)]
119. Wang, Y.; Cheng, W.; Yuan, P.; Yang, G.; Mu, S.; Liang, J.; Xia, H.; Guo, K.; Liu, M.; Zhao, S.; et al. Boosting Nitrogen Reduction to Ammonia on FeN₄ Sites by Atomic Spin Regulation. *Adv. Sci.* **2021**, *8*, 2102915. [[CrossRef](#)]
120. Liang, Y.; Banjac, K.; Martin, K.; Zigon, N.; Lee, S.; Vanthuyne, N.; Garcés-Pineda, F.A.; Galán-Mascarós, J.R.; Hu, X.; Avarvari, N.; et al. Enhancement of electrocatalytic oxygen evolution by chiral molecular functionalization of hybrid 2D electrodes. *Nat. Commun.* **2022**, *13*, 3356. [[CrossRef](#)]
121. Ma, Q.; Mu, S. Acidic oxygen evolution reaction: Mechanism, catalyst classification, and enhancement strategies. *Interdiscip. Mater.* **2023**, *2*, 53–90. [[CrossRef](#)]

Disclaimer/Publisher's Note: The statements, opinions and data contained in all publications are solely those of the individual author(s) and contributor(s) and not of MDPI and/or the editor(s). MDPI and/or the editor(s) disclaim responsibility for any injury to people or property resulting from any ideas, methods, instructions or products referred to in the content.